

Matching Layer Deposition for an Open-Source Ultrasound Tomography System: Inter-Element Variation in Frequency Response

Morgan Roberts*, Eleanor Martin, Michael Brown, Ben Cox, Bradley Treeby
Department of Medical Physics and Biomedical Engineering, University College London, UK

*Email: morgan.roberts.18@ucl.ac.uk

Abstract—Progress towards fast accurate Ultrasound Tomography (UST) requires experimental validation of new methods, creating a need for low-cost UST hardware, which can be achieved using in-house manufacture. However, a key challenge for transducer manufacture is controlling the composition and thickness of matching layers. For this work, a new low-cost deposition technique was developed, which is part of the **open-UST** manufacturing framework. To assess the technique, 8 16-element UST transducer modules were built, and the inter-element variation in their electrical input impedance, impulse response, and transmit-receive response was measured. The acoustic performance was highly uniform with no defective elements. The -40 dB transmit-receive bandwidth was 146 %, with a mean SNR of 60.5 dB, and the standard deviation in amplitude at the 1.21 MHz fundamental frequency, was very low $\sigma = \pm 7.1$ %, without using normalisation. The high uniformity is significant, because it means that the elements can be assumed to be identical during image reconstruction, which simplifies the assumptions required, and removes the need for extensive hydrophone calibration. The open-UST manufacturing framework could therefore lower the barrier to entry for researchers, and accelerate preliminary UST research.

Index Terms—tomography, transducer, open-source, low-cost

I. INTRODUCTION

Breast cancer screening reduces mortality, but mammograms have lower sensitivity for people with high breast density [1], and over-diagnosis causes harm in healthy people [2]. Ultrasound Tomography (UST) is an emerging but promising modality that produces sound-speed and acoustic-absorption distributions in breast tissue, which are useful biomarkers for classifying tissue types [3]. UST is also non-ionising, requires no painful breast compression, and is cheaper than MRI.

Initial clinical performance has been promising [4], but widespread adoption requires shorter acquisition and reconstruction times, while maintaining accuracy. Work towards this goal requires experimental validation of new methods, but there is a high barrier to entry for researchers starting UST experiments, since UST hardware is not available off the shelf, and custom systems are expensive.

This work was supported by the National Physical Laboratory, European Union's Horizon 2020 research and innovation programme H2020 ICT 2016-2017 under Grant Agreement No. 732411 (as an initiative of the Photonics Public Private Partnership), the Engineering and Physical Sciences Research Council (EPSRC), UK, Grant Nos. EP/S026371/1, and EP/P008860/1, and the EPSRC Centre For Doctoral Training in Intelligent Integrated Imaging In Healthcare (i4health).

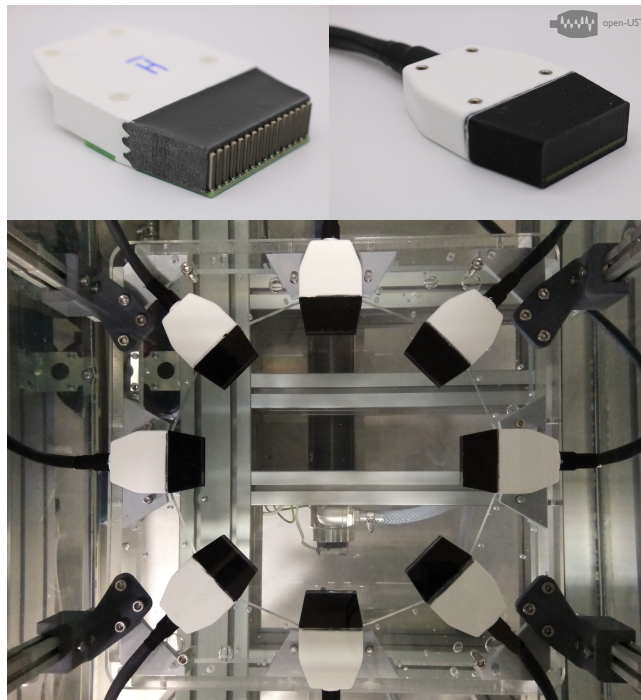


Fig. 1. **Top Left:** Transducer module after backing layer casting. **Top Right:** Finished transducer module. **Bottom:** 8 modules in a 2D ring array configuration.

To address this, the **open-UST** [5] project is being developed to support the in-house manufacture of UST research systems. The open-source hardware distribution includes CAD models, PCB and 3D-printing files, a bill of materials, assembly videos, and documentation of manufacture procedures. The standard open-UST configuration is a 220 mm 256-element 2D ring array, constructed from 16 linear modules, shown in Figure 1. The material cost is low (\sim £2,500 excluding DAQ hardware), and the manufacture does not require specialist equipment. At UCL, half of a standard open-UST array has been manufactured for testing, shown in Figure 1, comprising 8 transducer modules (128 elements). The second half is currently being manufactured.

The unique acoustic behaviour of each transducer element affects image reconstruction results [6]. Although a hydrophone calibration of each element could be used during

image reconstruction, this could present a new barrier-to-entry to researchers. Therefore, for open-UST transducers to be useful, the inter-element variation in acoustic performance must be low, so that transducer elements can be assumed to be identical during image reconstruction. A key transducer component affecting acoustic performance is the matching layer, and so the composition and thickness of this layer should be well controlled. For this work, a low-cost matching layer deposition technique was developed, and the inter-element variation in frequency response was assessed for 128 transducer elements.

II. ACOUSTIC MATCHING LAYER

A. Background

Matching layers can be manufactured by casting an excess of metal-polymer composite onto PZT elements, and then lapping the cured layer to the correct thickness [7], which requires specialist equipment to produce uniform, flat layers. Alternatively, the PZT can be bonded to a sheet material of a known thickness [8], but this requires specialist dispensing and pick-and-place equipment to achieve a thin, parallel bond line, especially for small element sizes. Instead, the matching layer can be cast close to the correct thickness without lapping. Previously, the transducer housing was used as a mould for casting a layer with a controlled thickness [9], but the housing became part of the acoustic stack, increasing attenuation. Therefore, a low cost technique to cast metal-polymer composites to the correct thickness is required.

Previously, prototype open-UST transducers were built to assess deposition techniques [10], resulting in a 16-element transducer module that demonstrated low inter-element variation in beamwidth and opening angle. However, the impulse response amplitudes varied widely before normalisation, and the deposition technique did not scale well to >16 elements, leading to the development of a new technique for this work.

B. Matching Layer Deposition

The new open-UST matching layer deposition process is shown in Figure 2, with supplementary details and photos available within the documentation [5].

Individual $10 \times 1 \times 1$ mm PZT bars (APC International) were cleaned by abrading the electrodes with P2000-grit Al_2O_3 sandpaper and degreasing with Isopropyl Alcohol. Two 1 mm glass coverslips (Corning) were cut to size and degreased, and a thin layer of release agent was applied to one side of each (Vaseline). A Polyvinyl Acetate (PVA) mould was 3D-printed to hold the elements during coating. First, the PVA mould was fixed to the glass base and PZT elements were loaded into the slots (Figure 2A). 3D-printed PLA standoffs were installed to set the coating blade height. Next, tungsten powder and epoxy resin were combined, with a tungsten mass ratio of 86.7%, on a glass mixing plate using a scraper for 20 minutes. The composite was then blade coated on top of the elements at a rate of ~ 0.6 mm/s, using a razor blade held at 45° with a 3D-printed PLA fixture (Figure 2B). The coating thickness was ~ 100 μm larger than the target matching layer

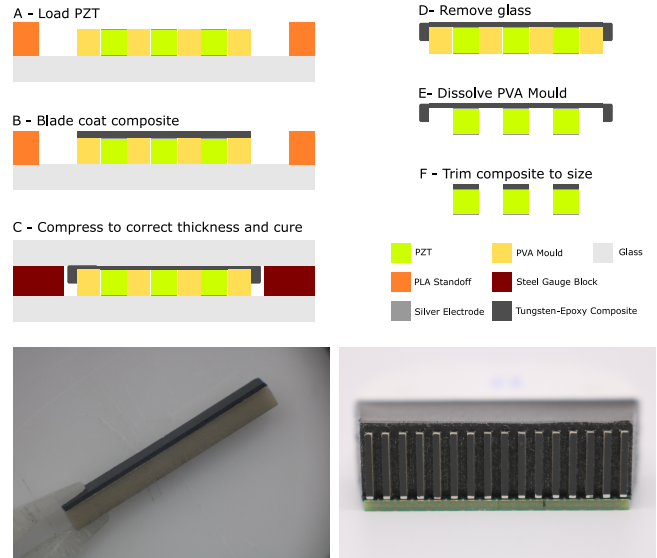


Fig. 2. **Top:** Matching layer deposition process. **Bottom Left:** Individual PZT bar with matching layer. **Bottom Right:** 16 matched elements bonded to a single backing layer, within a transducer module.

thickness. Next, the composite was compressed to the target thickness using the glass lid (Figure 2C). The glass plate spacing was set to $d_g = 1160$ μm using precision steel gauge blocks (M88, Kennedy). This distance is approximately equal to the target matched-PZT thickness $d_m = 1164$ μm , which is the sum of the mean unmatched-PZT thickness $d_p = 999$ μm (from Figure 3) and the target matching layer thickness $d_{qwm1} = 165$ μm . Compression was performed using a 3D-printed jig and machine screws to clamp the glass plates together. After curing, the glass was removed (Figure 2D) and the PVA mould was dissolved in water (Figure 2E). The composite was trimmed using a scalpel, producing individually matched PZT bars (Figure 2F). The remaining transducer assembly processes are described elsewhere [5], [10].

C. Matching Layer Thickness Variation

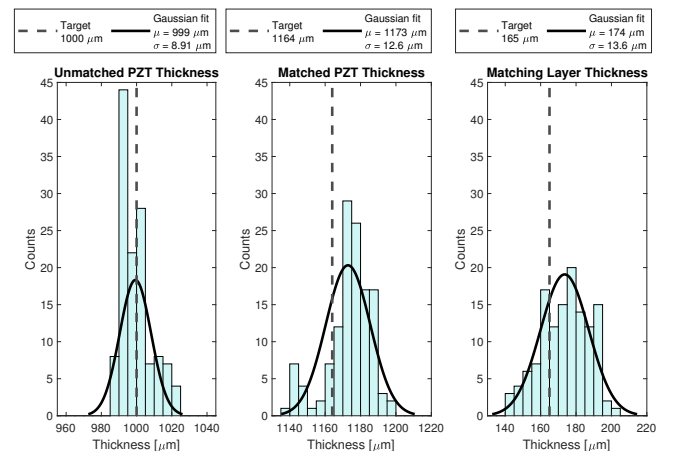


Fig. 3. Distribution of thickness measurements for $N = 128$ elements. **Left:** unmatched-PZT, **Middle:** matched-PZT, **Right:** matching layer only.

The thickness of the unmatched-PZT and the matched-PZT were measured using a digital micrometer (Mitutoyo 293-821-30), and the thickness of the matching layers was calculated, shown in Figure 3. The mean matched-PZT thickness was $1173 \mu\text{m}$, with a standard deviation of $12.6 \mu\text{m}$, and the mean matching layer thickness was $174 \mu\text{m}$, which is only $9 \mu\text{m}$ larger (+5 %) than the target value d_{qwml} . The matching layer thickness standard deviation was very low at $\sigma = 13.6 \mu\text{m}$ (8 % of d_{qwml}), which is only slightly larger than the variation in the unmatched-PZT thickness from the manufacturer ($\sigma = 8.91 \mu\text{m}$).

Figure 2 shows that the matched-PZT thickness should not exceed the thickness of the steel gauge block $d_g = 1160 \mu\text{m}$, but 87.5 % of the matched-PZT elements were thicker than this. There were problems compressing the composite due to its high viscosity. The high shear forces required were not achievable by clamping the glass plates, since they flexed and cracked. In future, thicker glass could be used, the clamping force could be spread over a larger area, and the blade coating thickness could be reduced. 12.5 % of the matched-PZT had a thickness less than d_g . This is because composite flowed through the gap between the PZT and the PVA mould, and underneath the PZT, lifting the elements up by $\sim 10 \mu\text{m}$. In future, this could be avoided by tuning the PVA mould slot width to be very close to the PZT width.

III. EXPERIMENTAL EVALUATION

A. Electrical Input Impedance

The electrical input impedance of 128 elements was measured for 100 frequencies between 0.4 MHz and 5 MHz, using a vector impedance analyser (HP 4193A), at two stages of the manufacture. The first measurement was made inside each transducer module, and is the impedance of the PCB traces and the backing-PZT-matching stack. The second measurement was made after cable installation, and is the transducer impedance modified by the cable. All measurements were performed with the transducer face immersed in degassed and deionised water at $21.7 \text{ }^\circ\text{C}$. Figure 4 shows the mean input impedance, and the range of the entire measured data. The mean series resonance frequency was 1.23 MHz with a very low standard deviation of 18 kHz . The magnitude and phase spectra for both measurement positions show good uniformity with no defective elements.

B. Transmit Impulse Response

The transmit impulse response of 64 elements was measured in degassed and deionised water at $22.1 \text{ }^\circ\text{C}$, with the modules connected to a Verasonics Vantage-256. The element-under-test was driven with a unipolar pulse (80 ns width, 90 V), and the impulse was measured in the far field at $z = 220 \text{ mm}$ using a $200 \mu\text{m}$ needle hydrophone (Precision Acoustics) connected to a digital oscilloscope (DPO5034B, Tektronix) via a submersible preamplifier and DC coupler (Precision Acoustics). For each element, the hydrophone was aligned with the beam axis using an X-Y stepper motor positioning system (Precision Acoustics). The frequency response of the

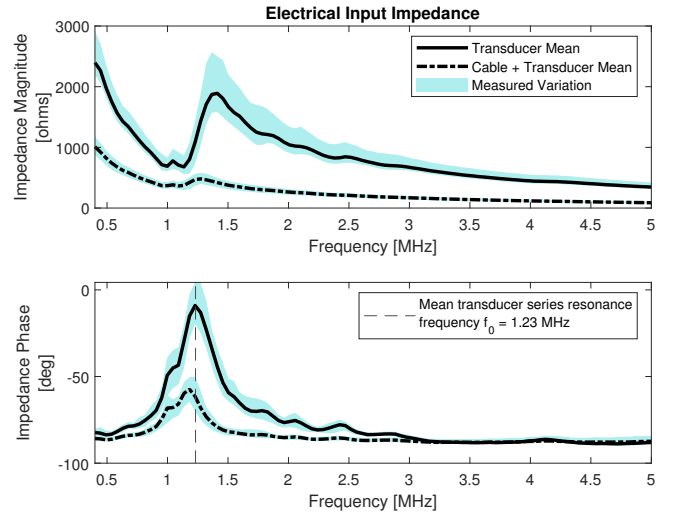


Fig. 4. Mean electrical input impedance spectra for $N = 128$ elements, measured at the transducer PCB (solid line), and at the cable input (dashed line). **Top:** impedance magnitude, **Bottom:** impedance phase.

hydrophone was deconvolved from the raw data, before band-pass filtering (300 kHz - 5 MHz). All of the signals were then aligned in time, and a Tukey window was applied before their amplitude spectra were calculated using a Fast Fourier Transform. Figure 5 shows the mean impulse response and amplitude spectrum, and the entire measured data.

The mean fundamental frequency was 1.22 MHz with a very low standard deviation of 22 kHz , which is consistent with the electrical input impedance spectra. The standard deviation in amplitude at the fundamental frequency was $\sigma = \pm 6.8 \%$ which is very low. No normalisation was used for these signals or their amplitude spectra.

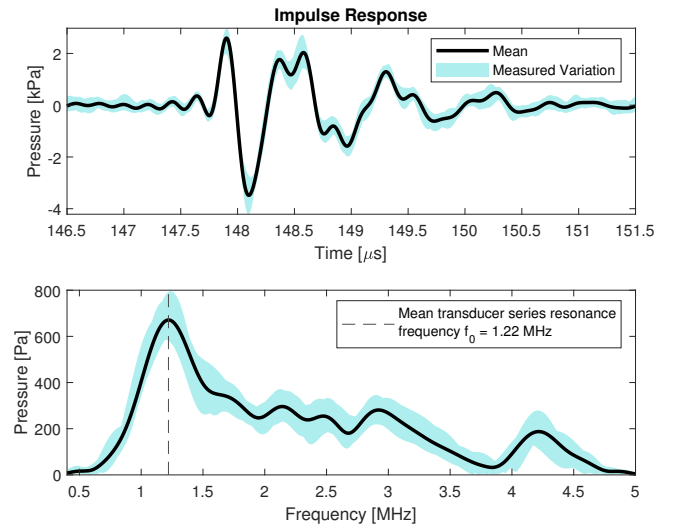


Fig. 5. Mean impulse response for $N = 64$ elements. **Top:** Measured hydrophone signals, aligned in time, **Bottom:** corresponding amplitude spectra.

C. Transmit-Receive Response

To measure the transmit-receive response of the transducer modules, they were assembled in a 2D ring array configuration, shown in Figure 1, and placed in a bath of degassed and deionised water at 22 °C, and connected to a Verasonics Vantage-256. For each transmit event the transmitting element was driven with a 1-cycle 1.20 MHz 80 V tri-state pulse, and receiver data was measured on the remaining 127 elements, without using averaging. This was repeated for all 128 transmitting elements, generating 16,256 received signals in total. Data from elements that were located $> 2.5^\circ$ from the transmitter beam axis were discarded, leaving 800 signals (~ 6 per transmitter). This was done because these signals should be similar, while off-axis receivers will detect a different pulse shape and amplitude, due to the frequency-dependent directional behaviour of the elements. The signals were aligned in time, and a Tukey window was applied before their amplitude spectra were calculated using a Fast Fourier Transform. Figure 6 shows the mean transmit-receive response and amplitude spectrum, and the range of the entire measured data. Again, no normalisation was used for these signals or their amplitude spectra. The mean fundamental frequency was 1.21 MHz with a very low standard deviation of 8.5 kHz, which is consistent with the electrical input impedance spectra and transmit impulse response. The standard deviation in amplitude at the fundamental frequency was $\sigma = \pm 7.1 \%$ which again is very low. The mean SNR of the $\pm 2.5^\circ$ receiver data was 60.5 dB, and at the -20 dB limit, the fractional bandwidth (825 kHz - 1.73 MHz) was 75 %. Although bandwidth is usually defined with a -6 dB limit, for full-waveform-inversion reconstruction methods it is common to generate a starting model using a low-pass filtered version of the data, where these frequency components can have amplitudes as low as -40 dB [11]. At the -40 dB limit, the fractional bandwidth (527 kHz - 2.29 MHz) was 146 %.

IV. DISCUSSION

A low-cost technique has been presented for depositing tungsten-epoxy matching layers onto PZT elements, as part of the open-source manufacturing framework, open-UST. This technique was tested for ($10 \times 1 \times 1$ mm) PZT bars, but could be easily adapted for larger elements, and for transducers for applications outside of UST.

Although there were problems with composite compression, it was shown that this manufacturing process still produced elements with very low inter-element variation in electrical input impedance, impulse response and transmit-receive response. This is significant, because it means that the elements can be assumed to be identical during image reconstruction, which simplifies the assumptions required. Next, characterisation of inter-element variation in beamwidth, opening angle, and beam axis skew will be performed for these transducers. Once the second half of the array has been manufactured, the full 256-element 16-module system will be used for phantom imaging experiments, to assess the feasibility of using low-cost hardware built in-house for ultrasound tomography work.

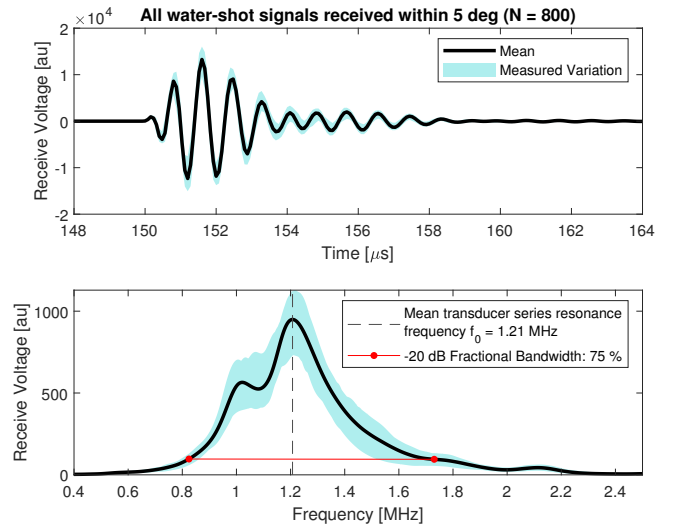


Fig. 6. Water-shot receiver data for $N = 128$ elements in a 2D ring array configuration. Receiver data from elements located $> 2.5^\circ$ from the transmitter beam axis were discarded. **Top:** Raw receiver data, shifted to align their minima, **Bottom:** corresponding amplitude spectra.

REFERENCES

- [1] H. D. Nelson, E. S. O'meara, K. Kerlikowske, S. Balch, and D. Miglioretti, "Factors associated with rates of false-positive and false-negative results from digital mammography screening: an analysis of registry data," *Annals of internal medicine*, vol. 164, no. 4, pp. 226–235, 2016.
- [2] M. G. Marmot, D. Altman, D. Cameron, J. Dewar, S. Thompson, and M. Wilcox, "The benefits and harms of breast cancer screening: an independent review," *British journal of cancer*, vol. 108, no. 11, pp. 2205–2240, 2013.
- [3] B. Malik, J. Klock, J. Wiskin, and M. Lenox, "Objective breast tissue image classification using quantitative transmission ultrasound tomography," *Scientific reports*, vol. 6, no. 1, pp. 1–8, 2016.
- [4] J. Wiskin, B. Malik, D. Borup, N. Pirshafiey, and J. Klock, "Full wave 3d inverse scattering transmission ultrasound tomography in the presence of high contrast," *Scientific Reports*, vol. 10, no. 1, pp. 1–14, 2020.
- [5] M. Roberts, morganjroberts.github.io/open-UST, 2022.
- [6] C. Cueto, L. Guasch, J. Cudeiro, O. C. Agudo, T. Robins, O. Bates, G. Strong, and M.-X. Tang, "Spatial response identification enables robust experimental ultrasound computed tomography," *IEEE Transactions on Ultrasonics, Ferroelectrics, and Frequency Control*, vol. 69, no. 1, pp. 27–37, 2021.
- [7] C.-M. Wong, Y. Chen, H. Luo, J. Dai, K.-H. Lam, and H. L.-w. Chan, "Development of a 20-mhz wide-bandwidth pmn-pt single crystal phased-array ultrasound transducer," *Ultrasonics*, vol. 73, pp. 181–186, 2017.
- [8] M. Angerer, M. Zapf, B. Leyrer, and N. V. Rüter, "Semi-automated packaging of transducer arrays for 3d ultrasound computer tomography," in *2020 IEEE SENSORS*. IEEE, 2020, pp. 1–4.
- [9] Y. Kim, A. D. Maxwell, T. L. Hall, Z. Xu, K.-W. Lin, and C. A. Cain, "Rapid prototyping fabrication of focused ultrasound transducers," *IEEE transactions on ultrasonics, ferroelectrics, and frequency control*, vol. 61, no. 9, pp. 1559–1574, 2014.
- [10] M. Roberts, E. Martin, M. Brown, B. Cox, and B. Treeby, "Transducer module development for an open-source ultrasound tomography system," in *2021 IEEE International Ultrasonics Symposium (IUS)*, 2021, pp. 1–4.
- [11] J. Cudeiro-Blanco, C. Cueto, O. Bates, G. Strong, T. Robins, M. Toulemonde, M. Warner, M.-X. Tang, O. C. Agudo, and L. Guasch, "Design and construction of a low-frequency ultrasound acquisition device for 2-d brain imaging using full-waveform inversion," *Ultrasound in Medicine & Biology*, vol. 48, no. 10, pp. 1995–2008, 2022.